SCIENCE CHINA
Information Sciences

• RESEARCH PAPER • doi: 10.1007/s11432-012-4683-7

A unified level set framework utilizing parameter priors for medical image segmentation

WANG LingFeng[1*], YU ZeYun[2] & PAN ChunHong[1]

[1]*National Laboratory of Pattern Recognition (NLPR), Institute of Automation, Chinese Academy of Sciences, Beijing* 100190, *China;*
[2]*Department of Computer Science, University of Wisconsin-Milwaukee, USA*

Received May 11, 2011; accepted April 2, 2012

Abstract Image segmentation plays an important role in many medical imaging systems, yet in complex circumstances it remains an open problem. One of the main difficulties is the intensity inhomogeneity in an image. In order to tackle this problem, we first introduce a region-based level set segmentation framework to unify the traditional global and local methods. We then propose two novel parameter priors, i.e., the local order regularization and interactive regularization, and then utilize them as the constraints of the objective energy function. The objective energy function is finally minimized via a level set evolution process to achieve image segmentation. Extensive experiments show that the proposed approach has gained significant improvements in both accuracy and efficiency over the state-of-the-art methods.

Keywords image segmentation, level set, local order regularization, interactive regularization

Citation Wang L F, Yu Z Y, Pan C H. A unified level set framework utilizing parameter priors for medical image segmentation. Sci China Inf Sci, 2012, 55, doi: 10.1007/s11432-012-4683-7

1 Introduction

Image segmentation is a key process in various medical imaging systems and a fundamental step for subsequent tasks such as feature recognition and scene understanding. However, the performance of segmentation is largely influenced by many factors. One of the major problems arises from the image intensity inhomogeneity, which is the focus of the present work.

1.1 Related work

Recently, level set model has been extensively applied to medical image segmentation because of several of its desirable advantages over traditional image segmentation methods. First, it can achieve sub-pixel segmentation accuracy on object boundaries. Second, it can naturally handle the topology change of the contours. Existing level set methods can be broadly classified into two groups: i.e., edge-based methods [1–3] and region-based methods [4–19]. The edge-based methods utilize local edge information to attract the active contour toward the object boundaries. These methods have two inevitable limitations [4]: dependence on the initial contour and sensitivity to image noise. The region-based methods, on the other

*Corresponding author (email: lfwang@nlpr.ia.ac.cn)

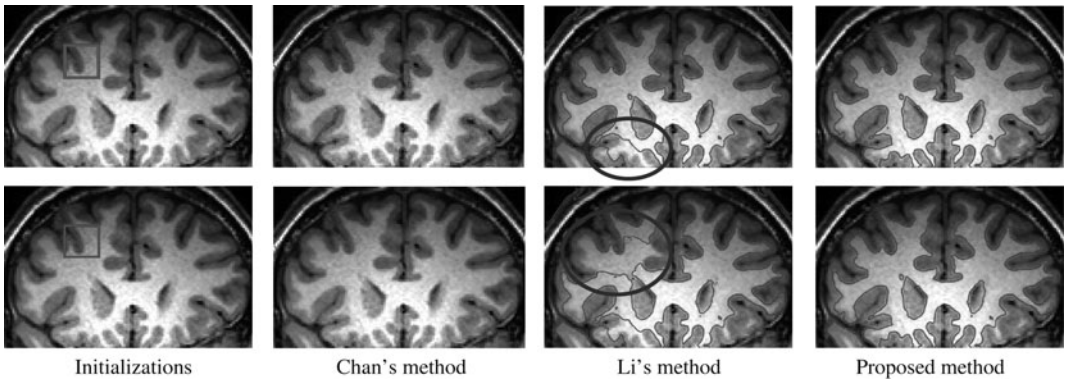

Figure 1 A comparison of the proposed method to the traditional methods, including Chan's method [4] (a global method) and Li's method [8] (a local method). Note that, two different yet very similar initial contours are used to test the sensitivity to initialization.

hand, are introduced to overcome the two limitations. These methods identify each region of interest by a certain region descriptor, such as intensity, to guide the evolution of the active contour. However, these methods tend to rely on the assumption of homogeneity of the region descriptor. The region-based segmentation methods can be further classified into two subgroups: i.e., global methods [4–6,10–13] and local methods [7–9,14–19].

One of the most popular global methods is proposed by Chan et al. [4]. This method first assumes that image intensities are statistically homogeneous in each segmented region. Then, it utilizes the global objective energy function to represent this homogeneity. Some variants of the global method have been reported in [4–6]. However, the details of the object always cannot be correctly segmented out by these methods. Also, these methods cannot effectively tackle the intensity inhomogeneity problem (for example, see Figure 1). The local methods are proposed to address the intensity inhomogeneity. These methods assume that the intensities in a relatively small local region are separable. Li et al. [8] introduce a local fitting energy due to a kernel function, which is used to extract the local image information. Motivated by [8], the local Gaussian distribution fitting energy and the local image fitting energy are proposed in [9] and [16], respectively. An et al. [7] offered a variational region-based algorithm, which combines the convergence approximation with a new multi-scale piecewise smooth model. These algorithms have some advantages in dealing with the intensity inhomogeneity problem over the global methods. Unfortunately, these local methods are also sensitive to the initial contour and the segmentation results are not accurate enough in some cases. As shown in Figure 1, although the two initial contours are very similar, the segmentation results by [8] are quite different. Furthermore, both results have obvious false contours (indicated by the ellipses). The main reason for these two problems is that the prior on local intensity clusters is ignored in these local methods. As will be shown in our unified framework below, only the contour prior is used in these methods.

1.2 The proposed method

Our work is mainly motivated by the traditional region-based level methods [4,7,8] and the interactive segmentation methods [20–23]. In this work, we propose two novel parameter regularizations, the key points in our proposed unified segmentation framework, to tackle the intensity inhomogeneity problem. The advantages of the proposed method are listed below.

1. We propose a unified framework for region-based level set image segmentation. By using this framework, the traditional global and local segmentation methods can be represented by different energy terms utilized in the objective energy function. Furthermore, with this framework it is straightforward to find the drawbacks of the two traditional methods. That is, the global (strong) parameter regularization is used in the global methods and no parameter regularization is adopted in the local methods. It is also convenient to add other energy terms into our unified framework to enhance the result.

2. We propose two novel parameter regularizations, the local order regularization and interactive regularization, and incorporate them into the objective energy function. There are two benefits of using these regularizations. First, the local characteristic can soften the global constraint in the global methods. Second, using additional constraints can strengthen the stability of the local methods. Adding the local order regularization to the traditional local method, the detailed information can be accurately segmented out and the algorithm is insensitive to the initialization. By using the interactive regularization, the segmentation results can be user-controllable and significantly improved. That is, it is very easy to add the interactive information into the algorithm.

2 The unified framework

Let $\Omega \subset \mathbb{R}^2$ be the image domain, and let $\boldsymbol{I} : \Omega \to \mathbb{R}$ be the given gray-level medical image satisfying $\boldsymbol{I}_{\boldsymbol{x}} = \boldsymbol{I}(\boldsymbol{x})$, where $\boldsymbol{x} \in \Omega$. Level set methods formulate the image segmentation problem as finding a contour Γ, which splits Ω into two non-overlapping regions, i.e., the Ω^f and Ω^b, corresponding to the interior of Γ (foreground) and the exterior of Γ (background), respectively. For region-based level set segmentation methods, each pixel $\boldsymbol{I}_{\boldsymbol{x}}$ at location $\boldsymbol{x}$ is further modeled by two parameters, i.e., the $\boldsymbol{C}^f_{\boldsymbol{x}}$ and $\boldsymbol{C}^b_{\boldsymbol{x}}$, which correspond to foreground and background parameters. The proposed unified framework interprets the region-based level set segmentation problem as the Bayesian estimation of the contour Γ:

$$\Gamma = \arg\max_{\Gamma, \boldsymbol{C}^f, \boldsymbol{C}^b} p(\Gamma, \boldsymbol{C}^f, \boldsymbol{C}^b | \boldsymbol{I}), \tag{1}$$

where $\boldsymbol{C}^f$ and $\boldsymbol{C}^b$ are all foreground and background parameters, that is $\boldsymbol{C}^{f/b} = \{\boldsymbol{C}^{f/b}_{\boldsymbol{x}} | \boldsymbol{x} \in \Omega\}$. By Bayes' theorem, Eq. (1) can be rewritten as

$$\begin{aligned} \Gamma &= \arg\max_{\Gamma, \boldsymbol{C}^f, \boldsymbol{C}^b} p(\Gamma, \boldsymbol{C}^f, \boldsymbol{C}^b | \boldsymbol{I}) \\ &\propto \arg\max_{\Gamma, \boldsymbol{C}^f, \boldsymbol{C}^b} p(\boldsymbol{I} | \Gamma, \boldsymbol{C}^f, \boldsymbol{C}^b) p(\Gamma, \boldsymbol{C}^f, \boldsymbol{C}^b) \\ &\propto \arg\max_{\Gamma, \boldsymbol{C}^f, \boldsymbol{C}^b} p(\boldsymbol{I} | \Gamma, \boldsymbol{C}^f, \boldsymbol{C}^b) p(\Gamma) p(\boldsymbol{C}^f, \boldsymbol{C}^b), \end{aligned} \tag{2}$$

where the contour Γ and $\boldsymbol{C}^f$ and $\boldsymbol{C}^b$ are assumed to be independent of each other. The first term $p(\boldsymbol{I}|\Gamma, \boldsymbol{C}^f, \boldsymbol{C}^b)$ is the likelihood of the image, the second term $p(\Gamma)$ is the contour regularizing prior, and the last term $p(\boldsymbol{C}^f, \boldsymbol{C}^b)$ is the foreground/background parameter prior. The maximum a posteriori estimation in Eq. (2) is equivalent to minimizing the following objective function:

$$J(\Gamma) = L(\boldsymbol{I}, \Gamma, \boldsymbol{C}^f, \boldsymbol{C}^b) + \mu R_c(\Gamma) + \nu R_p(\boldsymbol{C}^f, \boldsymbol{C}^b), \tag{3}$$

where μ, ν are two weighting constants, $L(.)$ is the likelihood item, $R_p(.)$ is the parameter regularization item, and $R_c(.)$ is the contour regularization item. The weighting parameters μ and ν are used to balance the likelihood and two priors. That is, a larger μ will result in smoother segmented contours. But some detailed information may be lost, especially on weak edges. On the contrary, a smaller μ will decrease the smoothness of the segmented contours. But some image details can be well segmented. In our implementation, the weighting constant μ is adaptively set according to the image size. Similarly, a larger ν holds the local order or interactive information better, but leading to a loss in more details. In our implementation, the foreground/background parameter prior $R_p(\boldsymbol{C}^f, \boldsymbol{C}^b)$ is regarded as a hard constraint. Hence, we do not need to specify the weighting constant ν beforehand in our method.

2.1 Traditional global methods

For the traditional global methods (see, e.g., [4]), the parameter prior is simply interpreted as the two following global constants:

$$R_p(\boldsymbol{C}^f, \boldsymbol{C}^b) = R^f_p(\boldsymbol{C}^f) + R^b_p(\boldsymbol{C}^b), \tag{4}$$

where $R_p^f(\boldsymbol{C}^f)$ and $R_p^b(\boldsymbol{C}^b)$ are defined as

$$R_p^\bullet(\boldsymbol{C}^\bullet) = \int_{\boldsymbol{x}\in\Omega^\bullet} \left\|\boldsymbol{C}_{\boldsymbol{x}}^\bullet - c^\bullet\right\|^2 \mathrm{d}\boldsymbol{x}, \text{ where } \bullet \in \{f, b\}, \tag{5}$$

in which c^f and c^b are two unknown constants. The parameter regularization item used in global method requires that (see Eqs. (4) and (5)) foreground parameter in Ω^f should be close to the constant c^f, while background parameter in Ω^b should be close to the constant c^b. The contour regularization is always interpreted as the contour length, the interior region area, and other contour smoothness items. In [4], two items, namely, the contour length and the interior region area, are utilized as the contour regularization, that is,

$$R_c(\Gamma) = \alpha \oint_\Gamma \mathrm{d}s + \beta \int_{\boldsymbol{x}\in\Omega_f} \mathrm{d}\boldsymbol{x}. \tag{6}$$

The likelihood term measures the conformity of image data within the interior and exterior regions:

$$L(\boldsymbol{I}, \Gamma, \boldsymbol{C}^f, \boldsymbol{C}^b) = \sum_{\bullet\in\{f,b\}} \int_{\boldsymbol{x}\in\Omega_\bullet} \|\boldsymbol{I}_{\boldsymbol{x}} - \boldsymbol{C}_{\boldsymbol{x}}^\bullet\|^2 \mathrm{d}\boldsymbol{x}. \tag{7}$$

In [4], the parameter regularization is used as the hard constraint. Therefore, combining (7) with (4) and (5), the likelihood term Eq. (7) is reformulated as

$$L(\boldsymbol{I}, \Gamma, \boldsymbol{C}^f, \boldsymbol{C}^b) = \sum_{\bullet\in\{f,b\}} \int_{\boldsymbol{x}\in\Omega_\bullet} \|\boldsymbol{I}_{\boldsymbol{x}} - c^\bullet\|^2 \mathrm{d}\boldsymbol{x}. \tag{8}$$

The specified two constants c^f and c^b globally govern all the pixel intensities in Ω^f and Ω^b, respectively. Furthermore, the two constants c^f and c^b can be interpreted as the cluster centers, i.e., the foreground cluster c^f and the background cluster c^b.

2.2 Traditional local methods

The traditional local methods neglect the parameter regularization [8], and their contour regularization is same as that of the global methods. The main difference between the local and global methods lies in how to represent likelihood. The local methods describe the likelihood term using a kernel function

$$L(\boldsymbol{I}, \Gamma, \boldsymbol{C}^f, \boldsymbol{C}^b) = \int E(\Gamma, \boldsymbol{C}_{\boldsymbol{x}}^f, c_{\boldsymbol{x}}^b) \mathrm{d}\boldsymbol{x} = \int E(\boldsymbol{x}) \mathrm{d}\boldsymbol{x}, \tag{9}$$

where $E(\boldsymbol{x})$ is the local fitting energy [8] defined as

$$E(\boldsymbol{x}) = \sum_{\bullet\in\{f,b\}} \int_{\boldsymbol{x}\in\Omega_\bullet} K_\sigma(\boldsymbol{x} - \boldsymbol{y}) \|\boldsymbol{I}_{\boldsymbol{y}} - \boldsymbol{C}_{\boldsymbol{x}}^\bullet\|^2 \mathrm{d}\boldsymbol{x}, \tag{10}$$

where $K_\sigma(\cdot)$ is the Gaussian function: $K_\sigma(\boldsymbol{x}) = \frac{1}{(2\pi)^{n/2}\sigma^n} e^{-\|\boldsymbol{x}\|^2/2\sigma^2}$; $\boldsymbol{C}_{\boldsymbol{x}}^f$ and $\boldsymbol{C}_{\boldsymbol{x}}^b$ are locally calculated by the pixel intensities centered at position $\boldsymbol{x}$, whose size is controlled by σ. Similarly, $\boldsymbol{C}_{\boldsymbol{x}}^f$ and $\boldsymbol{C}_{\boldsymbol{x}}^b$ can be further interpreted as two local cluster centers at position $\boldsymbol{x}$.

To sum up, the main difference between the traditional global and local methods lies in the choice of cluster centers. The global-homogenous method simply utilizes two constants c^f and c^b as the cluster centers, and formulates it as the global likelihood term expressed in (8). By contrast, the local-homogenous method adopts the local cluster centers $\boldsymbol{C}_{\boldsymbol{x}}^f$ and $\boldsymbol{C}_{\boldsymbol{x}}^b$ at each location $\boldsymbol{x}$, and formulates it as the local likelihood term expressed in (9).

3 Local priors

Intensity inhomogeneity is a common problem in many medical images. The local methods perform better than the global ones in finding accurate feature boundaries. However, the local methods also have some

problems—they often ignore the parameter prior. If only the likelihood and contour regularization terms (without parameter regularization term) are used to represent the objective energy function Eq. (3), this objective function will have many local optimal solutions, yielding two problems: (i) the solution is sensitive to the initialization, and (ii) the segmentation result has some obvious errors. As described in Subsection 2.1, the global methods utilize the regularization term (see Eqs. (4) and (5)). Unfortunately, the global constraint used in these methods is so strong that it is hard to meet the inhomogeneity property in a medical image. Thus, a reasonable solution is adding parameter regularization as the constraint to the local methods. In the rest of this section, we first propose two parameter regularizations, i.e., the local order regularization and the interactive regularization. We then present the corresponding objective energy function.

3.1 Local order regularization

In a medical image, the intensity values often manifest local order, meaning that the foreground (target) intensity values are statistically larger (or smaller) than the background (non-target) in a relative small local region. Take the Figure 1 as an example; the intensity values in foreground (such as the write matter) are greater than those in background (such as the gray matter) in a small local region. Thus, the foreground cluster center value $\boldsymbol{C}_{\boldsymbol{x}}^f$ is larger than the background cluster center value $\boldsymbol{C}_{\boldsymbol{x}}^b$ at each location $\boldsymbol{x}$. With this in mind, we propose the local order regularization to represent the local order information as follows:

$$R_p(\boldsymbol{C}^f, \boldsymbol{C}^b) = \int_{\boldsymbol{x}\in\Omega} s(\boldsymbol{C}_{\boldsymbol{x}}^b - \boldsymbol{C}_{\boldsymbol{x}}^f)\mathrm{d}\boldsymbol{x}, \tag{11}$$

where $s(\cdot)$ is the sign function:

$$s(x) = \begin{cases} 1, & x > 0, \\ 0, & x = 0, \\ -1, & x < 0. \end{cases}$$

Note that the order constraint interpreted in Eq. (11) requires that the local foreground cluster $\boldsymbol{C}_{\boldsymbol{x}}^f$ should be larger than local background cluster $\boldsymbol{C}_{\boldsymbol{x}}^b$. If we want to keep $\boldsymbol{C}_{\boldsymbol{x}}^f$ smaller than $\boldsymbol{C}_{\boldsymbol{x}}^b$, then Eq. (11) is reformulated as

$$R_p(\boldsymbol{C}^f, \boldsymbol{C}^b) = \int_{\boldsymbol{x}\in\Omega} s(\boldsymbol{C}_{\boldsymbol{x}}^f - \boldsymbol{C}_{\boldsymbol{x}}^b)\mathrm{d}\boldsymbol{x}. \tag{12}$$

In the following, we only consider the first case in Eq. (11). Eq. (12) can be calculated similarly.

3.2 Interactive regularization

To reduce the intrinsic ambiguity in an image with complex features, an interactive environment may be designed to allow users to specify the foreground and background. However, the interactive framework is rarely used in the traditional region-based level set segmentation methods (both globally and locally), partly because it is hard to effectively incorporate the user guidance into these methods. With the unified framework discussed above, the incorporation becomes very straightforward by simply regarding the user inputs as the parameter regularization.

Let $\boldsymbol{X}^f$ and $\boldsymbol{X}^b$ be the location sets belonging to the user-specified foreground and background. The interactive results can be interpreted as two image intensity sets: the foreground set $\mathcal{F} = \{\boldsymbol{I}_{\boldsymbol{x}}^f | \boldsymbol{x} \in \boldsymbol{X}^f\}$ and the background set $\mathcal{B} = \{\boldsymbol{I}_{\boldsymbol{x}}^b | \boldsymbol{x} \in \boldsymbol{X}^b\}$, which contain the user specified foreground pixels and background pixels, respectively.

In our method, the thresholding nearest neighbor model is adopted to represent the interactive regularization, although other more advanced yet complicated models may be used too. For each pixel at $\boldsymbol{x}$, let $\widehat{\boldsymbol{I}}_{\boldsymbol{x}}^f$ be the nearest pixel in the foreground set $\mathcal{F}$ and let $r_{\boldsymbol{x}}^f$ be the corresponding distances. Similarly, denote the nearest pixel in $\mathcal{B}$ by $\widehat{\boldsymbol{I}}_{\boldsymbol{x}}^b$ and the corresponding distance by $r_{\boldsymbol{x}}^b$. The definition of the interactive regularization is expressed as

$$R_p(\boldsymbol{C}^f, \boldsymbol{C}^b) = \int_{\boldsymbol{x}\in\Omega} \sum_{\bullet\in\{f,b\}} \big(t_\tau(r_{\boldsymbol{x}}^\bullet)(\boldsymbol{C}_{\boldsymbol{x}}^\bullet - \widehat{\boldsymbol{I}}_{\boldsymbol{x}}^\bullet)\big)\mathrm{d}\boldsymbol{x}, \tag{13}$$

where $t_\tau(\cdot)$ is the τ-thresholding function (threshold is τ),

$$t_\tau(x) = \begin{cases} 1, & x < \tau, \\ 0, & \text{else.} \end{cases}$$

In our implementation, we set $\tau = 5$. By Eq. (13), for the pixel at $\boldsymbol{x}$, if its distance to the nearest pixel $\widehat{\boldsymbol{I}}^f_{\boldsymbol{x}}$ in the foreground set $\mathcal{F}$ is smaller than τ, then its foreground parameter $\boldsymbol{C}^f_{\boldsymbol{x}}$ should be as close to the nearest foreground pixel $\widehat{\boldsymbol{I}}^f_{\boldsymbol{x}}$ as possible. The same interpretation applies to the background set $\mathcal{B}$.

3.3 Energy formulation

By incorporating the local likelihood term (Eq. (9)), the contour regularization term (the first term in Eq. (6)), and the parameter regularization term (Eq. (11)) into Eq. (3), we get the final objective energy function as follows:

$$J_{\text{order}}(\Gamma) = \int E(\boldsymbol{x})\mathrm{d}\boldsymbol{x} + \mu \oint_\Gamma \mathrm{d}s + \nu \int_{\boldsymbol{x}\in\Omega} s(\boldsymbol{C}^b_{\boldsymbol{x}} - \boldsymbol{C}^f_{\boldsymbol{x}})\mathrm{d}\boldsymbol{x}. \tag{14}$$

Similarly, by adopting Eq. (13) as the parameter regularization term, we have the objective function that contains interactive user-guidance:

$$J_{\text{inter}}(\Gamma) = \int E(\boldsymbol{x})\mathrm{d}\boldsymbol{x} + \mu \oint_\Gamma \mathrm{d}s + \nu \int_{\boldsymbol{x}\in\Omega} \sum_{\bullet\in\{f,b\}} \big(t_\tau(r^\bullet_{\boldsymbol{x}})(\boldsymbol{C}^\bullet_{\boldsymbol{x}} - \widehat{\boldsymbol{I}}^\bullet_{\boldsymbol{x}})\big)\mathrm{d}\boldsymbol{x}. \tag{15}$$

4 Level set formulation and energy minimization

Level set formulation is performed to solve the above energy functions $J_{\text{order}}(\Gamma)$ and $J_{\text{inter}}(\Gamma)$. In this section, we describe the solution of $J_{\text{order}}(\Gamma)$ in detail. To get the solution of $J_{\text{inter}}(\Gamma)$, we only need to redefine the parameter regularization term. In level set methods, a contour Γ is represented by the zero level set of a Lipschitz function $\phi : \Omega \to \mathbb{R}$, called a level set function. Accordingly, the energy of our method can be defined as

$$\begin{aligned} F(\phi) \;=\; & \iint K_\sigma(\boldsymbol{x}-\boldsymbol{y})\|\boldsymbol{I}_{\boldsymbol{y}} - \boldsymbol{C}^f_{\boldsymbol{x}}\|^2 H(\phi(\boldsymbol{y}))\mathrm{d}\boldsymbol{y}\mathrm{d}\boldsymbol{x} + \iint K_\sigma(\boldsymbol{x}-\boldsymbol{y})\|\boldsymbol{I}_{\boldsymbol{y}} - \boldsymbol{C}^b_{\boldsymbol{x}}\|^2 \big(1 - H(\phi(\boldsymbol{y}))\big)\mathrm{d}\boldsymbol{y}\mathrm{d}\boldsymbol{x} \\ & + \mu Q(\phi) + \nu \int_{\boldsymbol{x}\in\Omega} s(\boldsymbol{C}^b_{\boldsymbol{x}} - \boldsymbol{C}^f_{\boldsymbol{x}})\mathrm{d}\boldsymbol{x} + \lambda P(\phi), \end{aligned} \tag{16}$$

where μ, ν, and λ are the weighting constants, $H(\cdot)$ is the Heaviside function, $Q(\phi) = \int \delta(\phi(\boldsymbol{x}))|\nabla\phi(\boldsymbol{x})|\mathrm{d}\boldsymbol{x}$ is the length term, $\delta(\cdot)$ is the derivative function of Heaviside function, and $P(\phi) = \int \frac{1}{2}(|\nabla\phi(\boldsymbol{x})| - 1)^2\mathrm{d}\boldsymbol{x}$. Note that the term $P(\phi)$ is another regularization term [9] used to maintain the regularity of the level set function. In our implementation, Heaviside function is approximated by a smooth function $H_\epsilon(x) = \frac{1}{2}\big[1 + \frac{2}{\pi}\arctan(\frac{x}{\epsilon})\big]$, and the corresponding derivative function $\delta_\epsilon(x)$ is defined by $\delta_\epsilon(x) = H'_\epsilon(x) = \frac{\epsilon}{\pi(\epsilon^2+x^2)}$. The parameter ϵ is chosen as 1.0 in our experiments.

The standard gradient descent method is performed to minimize the objective energy function $F(\phi)$ in two steps. In the first step, we fix the level set function ϕ, and calculate two cluster centers $\boldsymbol{C}^f_{\boldsymbol{x}}$ and $\boldsymbol{C}^b_{\boldsymbol{x}}$. In the second step, we fix the two cluster centers $\boldsymbol{C}^f_{\boldsymbol{x}}$ and $\boldsymbol{C}^b_{\boldsymbol{x}}$, and calculate the level set function ϕ. First, the variational method is utilized to calculate $\boldsymbol{C}^f$ and $\boldsymbol{C}^b$ for a fixed level set function ϕ as follows:

$$\boldsymbol{C}^f_{\boldsymbol{x}} = \max\big\{\widehat{\boldsymbol{C}}^f_{\boldsymbol{x}}, \widehat{\boldsymbol{C}}^b_{\boldsymbol{x}}\big\}, \quad \boldsymbol{C}^b_{\boldsymbol{x}} = \min\big\{\widehat{\boldsymbol{C}}^f_{\boldsymbol{x}}, \widehat{\boldsymbol{C}}^b_{\boldsymbol{x}}\big\}, \tag{17}$$

where $\widehat{\boldsymbol{C}}^f_{\boldsymbol{x}}$ and $\widehat{\boldsymbol{C}}^b_{\boldsymbol{x}}$ are defined as

$$\widehat{\boldsymbol{C}}^f_{\boldsymbol{x}} = \frac{K_\sigma(\boldsymbol{x}) \otimes \big[H_\epsilon(\phi(\boldsymbol{x}))\boldsymbol{I}_{\boldsymbol{x}}\big]}{K_\sigma(\boldsymbol{x}) \otimes H_\epsilon(\phi(\boldsymbol{x}))}, \quad \widehat{\boldsymbol{C}}^b_{\boldsymbol{x}} = \frac{K_\sigma(\boldsymbol{x}) \otimes \big[\big(1 - H_\epsilon(\phi(\boldsymbol{x}))\big)\boldsymbol{I}_{\boldsymbol{x}}\big]}{K_\sigma(\boldsymbol{x}) \otimes \big(1 - H_\epsilon(\phi(\boldsymbol{x}))\big)}, \tag{18}$$

in which $\otimes$ is the convolution operation. Note that, the local order energy is regarded as a hard constraint, which is represented by Eq. (17). The use of hard constraint is mainly based on the following two considerations: (i) we do not need to choose appropriate approximation sign function $s(\cdot)$; (ii) we do not need to decide the weighting constant ν.

Then, by keeping $\boldsymbol{C}^f$ and $\boldsymbol{C}^b$ fixed, the energy function is minimized with respect to the function ϕ based on the standard gradient descent by solving the following gradient flow equation:

$$\frac{\partial \phi}{\partial t} = -\delta_\epsilon(\phi)(\boldsymbol{T}^f - \boldsymbol{T}^b) + \mu\delta_\epsilon \mathrm{div}\left(\frac{\nabla\phi}{|\nabla\phi|}\right) + \lambda\left(\nabla^2\phi - \mathrm{div}\left(\frac{\nabla\phi}{|\nabla\phi|}\right)\right), \tag{19}$$

where $\boldsymbol{T}^f$ and $\boldsymbol{T}^b$ are defined as:

$$\boldsymbol{T}^\bullet(\boldsymbol{x}) = \int K_\sigma(\boldsymbol{y}-\boldsymbol{x})\|\boldsymbol{I}_{\boldsymbol{y}} - \boldsymbol{C}^\bullet_{\boldsymbol{x}}\|^2 \mathrm{d}\boldsymbol{y}, \quad \bullet \in \{f, b\}. \tag{20}$$

All the partial derivatives in Eq. (19) are simply discretized as the central finite differences, and the temporal derivative is discretized as a forward difference. The kernel K_σ is truncated as an $m \times m$ mask, where $m = 4\sigma + 1$. Our method proceeds in the following steps.

STEP_1. Initialize the level set function ϕ^0 by Eq. (21). In our implementation, we set $\rho = 2$.

$$\phi^0 = \phi(\boldsymbol{x}, t=0) = \begin{cases} -\rho, & \boldsymbol{x} \in \Omega_f - \partial\Omega_f, \\ 0, & \boldsymbol{x} \in \partial\Omega_f, \\ \rho, & \boldsymbol{x} \in \Omega - \Omega_f, \end{cases} \tag{21}$$

where $\partial\Omega_f$ is the boundary of Ω_f.

STEP_2. Calculate local clusters $\boldsymbol{C}^f_{\boldsymbol{x}}$ and $\boldsymbol{C}^b_{\boldsymbol{x}}$ from ϕ^n by Eqs. (17) and (18).

STEP_3. Evolve the level set function ϕ using Eq. (19). To obtain the numeric solution of Eq. (19), the current level set ϕ^{n+1} is updated by the previous iteration result ϕ^n, given by

$$\phi^{n+1} = \phi^n + \Delta t \frac{\partial \phi^n}{\partial t}, \tag{22}$$

where Δt is the time-step.

STEP_4. Repeat **STEP_2** and **STEP_3** until ϕ is converged or the maximum iteration number is reached.

When the interactive regularization is adopted as the parameter regularization, $J_{\mathrm{inter}}(\Gamma)$ should be used as the objective energy function. In this case, we only need to modify the calculations of the cluster centers $\boldsymbol{C}^f_{\boldsymbol{x}}$ and $\boldsymbol{C}^b_{\boldsymbol{x}}$. In other words, we need to rewrite Eq. (17) as

$$\boldsymbol{C}^f_{\boldsymbol{x}} = \frac{\widehat{\boldsymbol{C}}^f_{\boldsymbol{x}} + \nu t_\tau(r^f_{\boldsymbol{x}})\widehat{\boldsymbol{I}}^f_{\boldsymbol{x}}}{1 + \nu t_\tau(r^f_{\boldsymbol{x}})}, \quad \boldsymbol{C}^b_{\boldsymbol{x}} = \frac{\widehat{\boldsymbol{C}}^b_{\boldsymbol{x}} + \nu t_\tau(r^b_{\boldsymbol{x}})\widehat{\boldsymbol{I}}^b_{\boldsymbol{x}}}{1 + \nu t_\tau(r^b_{\boldsymbol{x}})}, \tag{23}$$

where $\widehat{\boldsymbol{I}}^f_{\boldsymbol{x}}$, $\widehat{\boldsymbol{I}}^b_{\boldsymbol{x}}$ and t_τ are defined in Subsection 3.2.

Convexity. As interpreted above, the local regularization term in Eq. (16) is used as the hard constraint. Hence, we only need to discuss the convexity of other terms. Formally, these terms are the same as those used in [8]. According to [24,25], the objective functional of [8] is non-convex. To sum up, our objective functional except the regularization term is non-convex, and thereby two-stage optimization method is adopted.

5 Experimental results

In this section, we demonstrate the advantages of our method, especially its robustness to the initialization and the segmentation accuracy. Unless otherwise specified, the coefficients are empirically set as follows: scale $\sigma = 3$, weighting constants $\lambda = 1$, $\nu = 1$, and $\mu = 0.004 \times h \times w$, where h and w are the height and width of the test image, and time-step $\Delta t = 0.1$. Meanwhile, we use convergence of level set or reaching max iteration as termination criterion. In our experiments, we set the max iteration number at a large

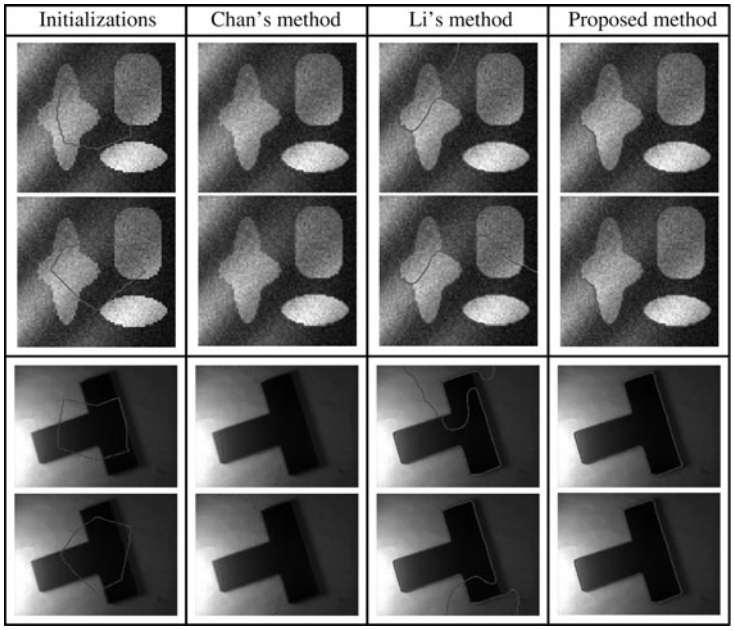

Figure 2 Visual comparison of our method with Chan's [4] and Li's methods [8]. From left to right are the initializations and the initialization results by Chan's, Li's, and our method, respectively. Two different initial contours are used to test the sensitivity to initialization.

value, i.e., 1000, to ensure that the level set converges before reaching the max iteration. The algorithms described are implemented with MATLAB and tested on a standard PC with a 2.4 GHz processor and 1024 MB of memory. A number of synthetic images as well as real medical images are used to evaluate the performance of the proposed scheme.

In the following, we shall first compare the traditional region-based level set segmentation methods with our method that utilizes the local order regularization. We then compare several other interactive segmentation methods with our method that utilizes the interactive regularization. And then, both regularizations will be combined in our method for comparison with other methods. Finally, we examine the influence of parameters of our method on the segmentation results.

5.1 Comparison with region-based methods

A number of experiments (on both synthetic images and real images) have been performed to evaluate the performance of the proposed scheme. We compare our method with the two representative region-based methods, i.e., the global method by Chan et al. [4][1)] and the local method by Li et al. [8][2)].

For the global method, the related parameters are listed as follows: weighting constant μ is set at $\mu = 0.002 \times 255$ and time-step $\Delta t = 0.1$. For the local method, the related parameters are as follows: scale $\sigma = 3$, weighting constants $\lambda = 1$, $\mu = 0.002 \times 255 \times 255$, and time-step $\Delta t = 0.1$. We use the same initializations in all methods for fair comparisons.

The results on two synthetic images are shown in Figure 2. Although images manifest intensity inhomogeneity, the feature boundaries are still accurately segmented out by our method, as compared to Chan's [4] and Li's [8] methods. Furthermore, the segmentation results of our method are less sensitive to the initialization than Li's method.

The comparisons on real images are illustrated in Figures 1 and 3 in detail. As shown in Figure 1, although the initialization contours are very similar, the segmentation results by Li's method have great difference, as well as significant errors. Moreover, the image details cannot be segmented out by Chan's method, since both images are inhomogeneous. On the other hand, the results of our method are not only very stable, but also very accurate. These experiments indicate that using parameter priors can

1) Available from: http://www.mathworks.com/matlabcentral/fileexchange/23445
2) Available from: http://www.engr.uconn.edu/∼cmli/

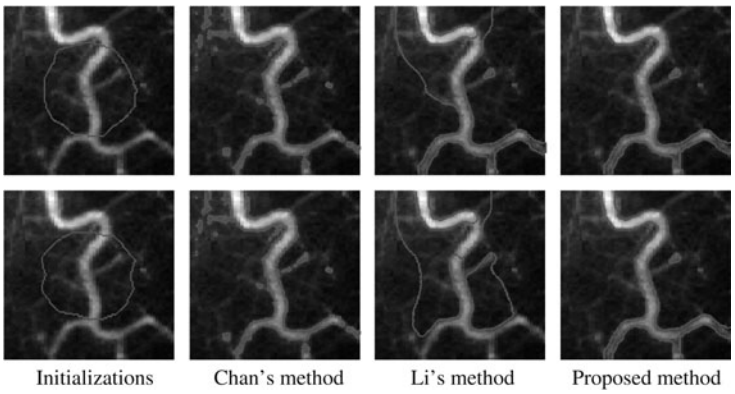

Figure 3 Visual comparison of our method with Chan's [4] and Li's methods [8]. From left to right are the initializations and the initialization results by Chan's, Li's, and our method, respectively. Two different initial contours are used to test the sensitivity to initialization.

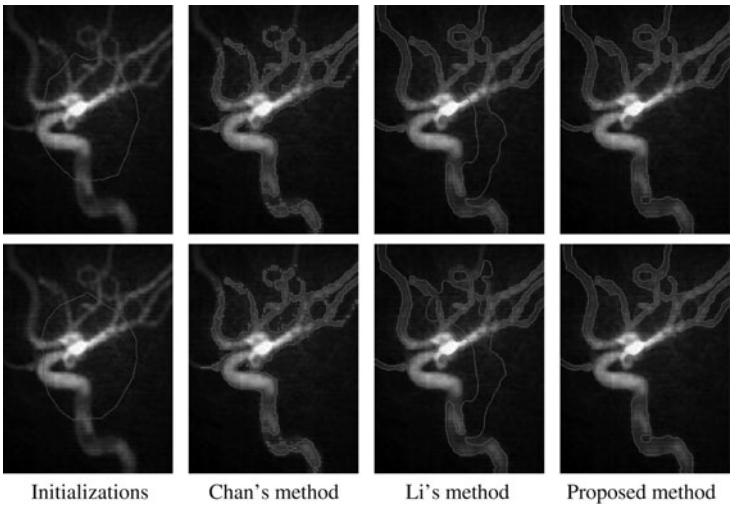

Figure 4 Visual comparison of our method with Chan's [4] and Li's methods [8] on a CTA image. From left to right are the initializations and the initialization results by Chan's, Li's, and our method, respectively. Two different initial contours are used to test the sensitivity to initialization.

improve segmentation accuracy of global method and at the same time strengthen the stability of the local method.

We also use three medial images with different acquisition techniques, such as CTA, X-ray, and MR, to evaluate our approach, and the comparison segmentation results are illustrated in Figures 4–6.

Although the acquisition techniques are different, our method can still segment the objects successfully. For example, the detailed information is correctly segmented in the 3T MR image, the weak boundaries are detected in the X-ray image, and the image inhomogeneous difficulty is tackled in the CTA image. Furthermore, the results of our method are robust to initialization.

5.2 Comparison with other interactive methods

In this subsection, we evaluate the proposed segmentation method (with interactive regularization) by comparing it with two traditional interactive segmentation methods, i.e., the random walk [21] and graph cut [20]. The source codes are downloaded from the author's home-page and run here for image segmentation. Different from the above experiments, the initial level set ϕ_{initial} is obtained by labeling the foreground and background masks. In order to segment the foreground accurately, we first use the local order regularization as the parameter regularization to obtain a rough contour. Then, the rough

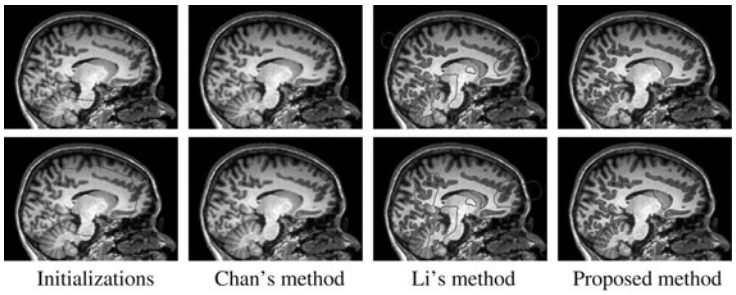

Figure 5 Visual comparison of our method with Chan's [4] and Li's methods [8] on a 3T MR image. From left to right are the initializations and the initialization results by Chan's, Li's, and our method, respectively. Two different initial contours are used to test the sensitivity to initialization.

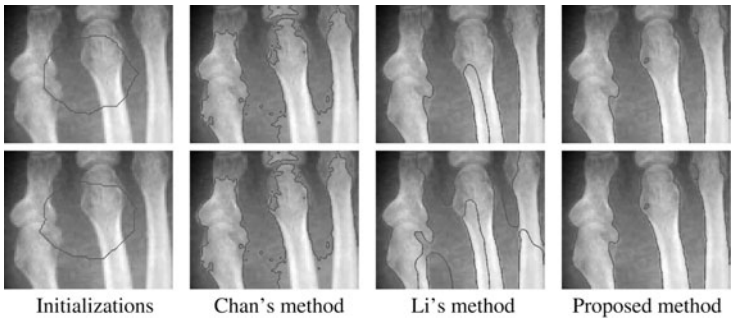

Figure 6 Visual comparison of our method with Chan's [4] and Li's methods [8] on an X-ray image. From left to right are the initializations and the initialization results by Chan's, Li's, and our method, respectively. Two different initial contours are used to test the sensitivity to initialization.

contour is treated as the initialization for the next segmentation process that uses the interactive regularization as the parameter regularization.

The visual comparisons are presented in Figure 7 and the computational costs on the two medical images are listed in Table 1. As illustrated in Figure 7, the detailed feature boundaries are lost in both random walk and graph cut algorithms, while our method produces better segmentation results. Moreover, as shown in Table 1, the computational cost of the graph cut algorithm increases significantly as the image resolution gets higher. Our method and the random walk algorithm are less expensive, especially for higher resolution images.

5.3 Combining two regularizations

In this subsection we shall combine the two regularizations in our method and compare the resultant method with the methods by Chan et al. [4] and Li et al. [8] and our algorithm that only uses local order regularization. To this end, we redefine $\boldsymbol{C}_{\boldsymbol{x}}^f$ and $\boldsymbol{C}_{\boldsymbol{x}}^b$ as follows:

$$\boldsymbol{C}_{\boldsymbol{x}}^f = \frac{\max\{\widehat{\boldsymbol{C}}_{\boldsymbol{x}}^f, \widehat{\boldsymbol{C}}_{\boldsymbol{x}}^b\} + \nu t_\tau(r_{\boldsymbol{x}}^f)\widehat{\boldsymbol{I}}_{\boldsymbol{x}}^f}{1 + \nu t_\tau(r_{\boldsymbol{x}}^f)}, \quad \boldsymbol{C}_{\boldsymbol{x}}^b = \frac{\min\{\widehat{\boldsymbol{C}}_{\boldsymbol{x}}^f, \widehat{\boldsymbol{C}}_{\boldsymbol{x}}^b\} + \nu t_\tau(r_{\boldsymbol{x}}^b)\widehat{\boldsymbol{I}}_{\boldsymbol{x}}^b}{1 + \nu t_\tau(r_{\boldsymbol{x}}^b)}. \tag{24}$$

The visual comparison of the segmentation results are shown in Figure 8. In the upper image, the object has some weak edges. If the initialization is not very good, the weak edge may not be segmented out only using local order regularization. Moreover, the lower image has a very undesirable background, and if we only use local order regularization, some background is segmented as object. On the other hand, the features are best segmented by combining the two regularizations. Thus, we can conclude that if the segmented image has weak edges or much undesirable background, adding interactive regularization is effectual.

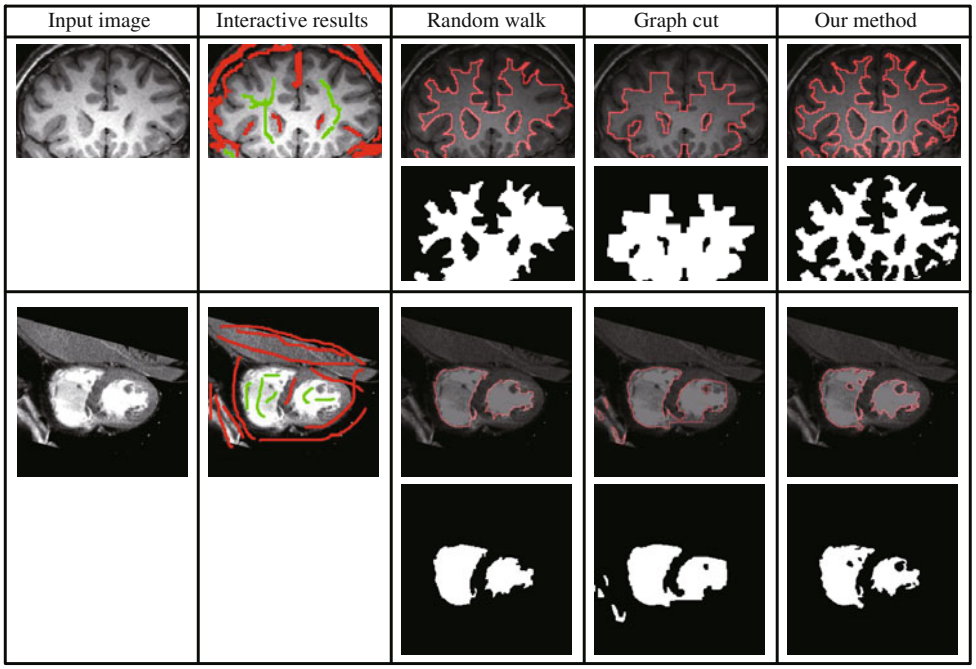

Figure 7 Two visual comparison of our method with two traditional interactive segmentation methods, namely the random walk and graph cut. The first and second columns are the source images and the user specified strokes about the foreground (in green) and background (in red). For each method, the upper row represents the segmented contours, while the lower row shows the segmented regions.

Table 1 The comparison of computational costs (unit: s)

Images	Resolution	Random walk	Graph cut	Ours
Image 1	119×78	1.11	1.43	0.44
Image 2	256×256	1.82	21.56	1.16

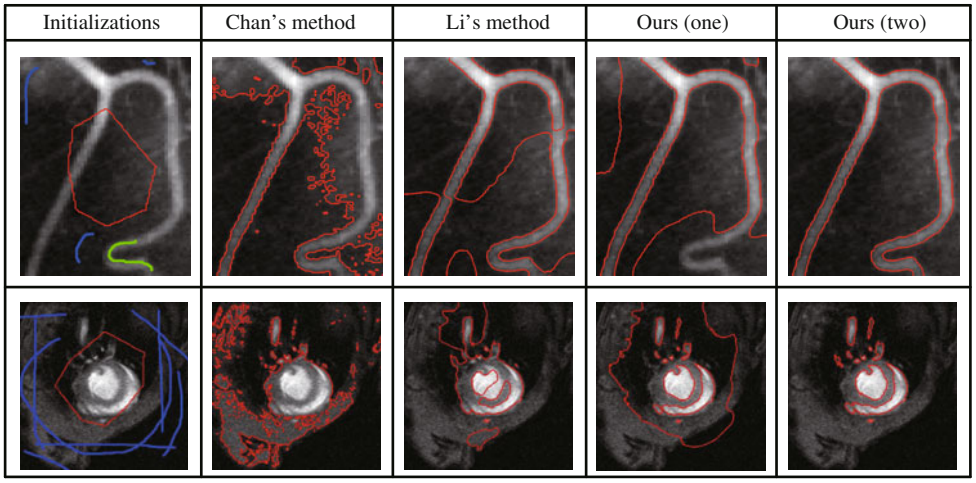

Figure 8 Visual comparison of our method with those of Chan's [4] and Li's [8] on two testing images. The first column is the user specified strokes about the foreground (in green) and background (in blue), and the initial contours (in red). Note that the method 'Our(one)' indicates the method that only uses the local order regularization, while the method 'Our(two)' represents the method that uses two regularizations.

Table 2 Comparisons by two error measures, i.e., the (FN) and (FP). 'Our(one)' is the method that only uses the local order regularization, while 'Our(two)' is the method that uses two regularizations

Scene	Chan		Li		Our (one)		our (two)	
	FN	FP	FN	FP	FN	FP	FN	FP
Scene 1	0.131	0.018	0.142	0.163	0.026	0.019	0.009	0.006
Scene 2	0.144	0.021	0.152	0.102	0.017	0.015	0.005	0.004
Scene 3	0.123	0.012	0.178	0.128	0.020	0.017	0.008	0.006
Scene 4	0.126	0.014	0.101	0.137	0.018	0.016	0.008	0.007
Scene 5	0.132	0.016	0.122	0.124	0.011	0.014	0.004	0.003
Scene 6	0.126	0.014	0.186	0.149	0.019	0.021	0.007	0.009

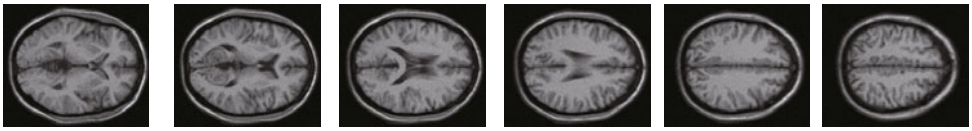

Figure 9 Images used in Table 2.

The numeric comparisons are presented in Table 2 (the tested images are shown in Figure 9). The tested simulated image sequences are downloaded from the BrainWeb[3)]. The segmentation results are compared with the ground truth by using the following two error measures: 1) false negative (FN), which calculates the ratio of foreground pixels that are missing over the ground truth; and 2) false positive (FP), which is the ratio of background pixels marked as foreground to the ground truth. Denoting by $R_{\text{target}}^{\text{our(one)}}$ the result of target region of 'our(one)' method. Similarly, by $R_{\text{in}}^{\text{chan}}$, $R_{\text{target}}^{\text{li}}$, $R_{\text{target}}^{\text{gt}}$ we denote Chan's, Li's, and ground truth. Thus, the FN and FP are defined as

$$\text{FP} = \frac{R_{\text{target}}^{*} - R_{\text{target}}^{*} \cap R_{\text{target}}^{\text{gt}}}{R_{\text{target}}^{\text{gt}}}, \quad \text{FN} = \frac{R_{\text{target}}^{\text{gt}} - R_{\text{target}}^{*} \cap R_{\text{target}}^{\text{gt}}}{R_{\text{target}}^{\text{gt}}}, \tag{25}$$

where $\{*|* \in \text{chan, li, our(one), our(two)}\}$. Note that, the ground truths in the BrainWeb are gray level image. To obtain the binary level ground truths, we perform thresholding operator on gray level images with threshold 128. As shown in Table 2, we select six different scenes. Both FN and FP of our methods are smaller than the traditional methods. That is to say, the proposed methods are of higher accuracy than the traditional methods. Furthermore, when using two regularizations, the two error measures are significantly reduced.

5.4 Analysis of the parameters

It is necessary to examine the influence of the parameters, such as weighting constant μ and the scale parameter σ, on the segmentation results, although the same scale parameter has been used for the previous images.

Figures 10 and 11 report the segmentation results of an MR image with different weighting constant μ and scale parameter σ, respectively, where all the segmentation results are very similar, meaning that our method is insensitive to parameters μ and σ to some extend. To sum up, with smaller scale or weighting constant, detailed boundary information can be better segmented, but with more noise edges. In contrast, the segmentation results are rather smooth.

6 Conclusions and future works

In this work, a unified region-based level set segmentation framework is presented. In particular, two

3) Available from: http://www.bic.mni.mcgill.ca/brainweb/

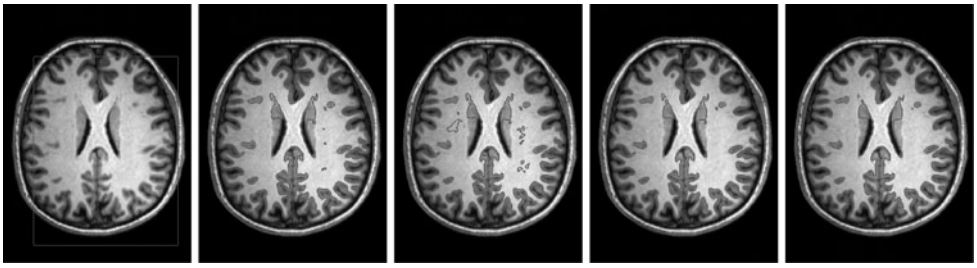

Figure 10 Results of our method with different weighting constant μ. From left to right are the initialization and the segmentation results with $\mu = \{0.002 \times h \times w, 0.004 \times h \times w, 0.006 \times h \times w, 0.008 \times h \times w\}$, respectively.

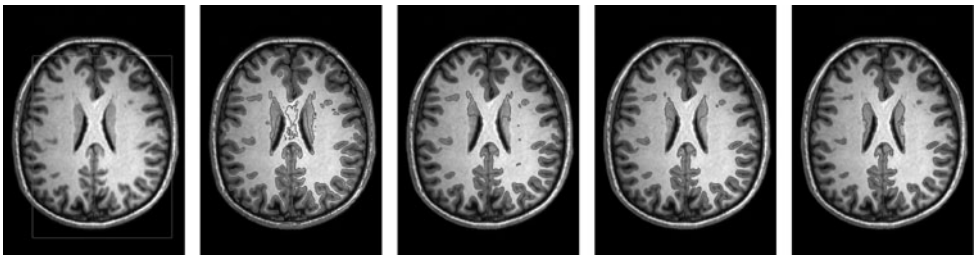

Figure 11 Results of our method with different scale σ. From left to right are the initialization and the segmentation results with $\sigma = \{1, 3, 5, 10\}$, respectively.

parameter regularizations, the local order regularization and interactive regularization, are introduced into this framework. Extensive experimental results demonstrate that the proposed method possesses the following two major advantages: 1) the feature boundaries in an image can be faithfully segmented; and 2) the method is insensitive to the initial contour. Although the present paper is focused on the demonstration of segmentation on medical images, the proposed algorithm can also be applied to other types of images, such as remote sensing images.

Although the proposed algorithm has the above advantages, it also has some shortcomings to be improved. For example, the objective energy functional except the regularization term is still non-convex, theoretically. Hence, our algorithm may rely on the initialization to some extent, although the initialization sensitive drawback in Li's [8] has been significantly improved. Note that, the non-convexity of objective functional is the common disadvantage of local region-based level set segmentation method. In practice, the proposed local order is a little rigid. Thus, this regularization is hardly applicable to the natural image segmentation problem, although it performs well in medical image. In our future work we will try to add some other regularization terms (such as the shape information) to further improve the segmentation performance and to handle more complex scenes. We are also planning to extend the proposed scheme to three-dimensional medical imaging data.

Acknowledgements

This work was supported by National Basic Research Program of China (Grant No. 2012CB316304) and National Natural Science Foundation of China (Grant Nos. 61175025, 61005036, 60975037).

References

1 Caselles V, Kimmel R, Sapiro G. Geodesic active contours. Int J Comput Vis, 1997, 22: 61–79

2 Yezzi A, Kichenassamy S, Kumar A, et al. A geometric snake model for segmentation of medical imagery. IEEE Trans Med Imaging, 1997, 16: 199–209

3 Li C, Xu C, Gui C, et al. Level set evolution without re-initialization: A new variational formulation. In: Proceedings of IEEE Conf on Computer Vision and Pattern Recognition. Los Alamitos: IEEE Computer Society Press, 2005. 430–436

4 Chan T F, Vese L A. Active contours without edges. IEEE Trans Image Process, 2001, 10: 266–277
5 Tsai A, Anthony Y J, Willsky A S. Curve evolution implementation of the mumfordcshah functional for image segmentation, de-noising, interpolation, and magnification. IEEE Trans Image Process, 2001, 10: 1169–1186
6 Vese L A, Chan T F. A multi-phase level set framework for image segmentation using the mumford and shah model. Int J Comput Vis, 2002, 50: 271–293
7 An J, Rousson M, Xu C. γ-convergence approximation to piecewise smooth medical image segmentation. In: Proceedings of Int Conf on Medical Image Computing and Computer Assisted Intervention (Part II). Berlin: Springer, 2007. 495–502
8 Li C, Kao C Y, Gore J C, et al. Minimization of region-scalable fitting energy for image segmentation. IEEE Trans Image Process, 2008, 17: 1940–1949
9 Wang L, Macione J, Sun Q, et al. Level set segmentation based on local gaussian distribution fitting. In: Proceedings of Asian Conf on Computer Vision. Berlin: Springer, 2009. 293–302
10 Liu H, Chen Y, Chen W. Neighborhood aided implicit active contours. In: Proceedings of IEEE Conference on Computer Vision and Pattern Recognition. Los Alamitos: IEEE Computer Society Press, 2006. 841–848
11 Lie J, Lysaker M, Tai X. A binary level set model and some applications to mumford-shah image segmentation. IEEE Trans Image Process, 2006, 15: 1171–1181
12 Ronfard R. Region-based strategies for active contour models. Int J Comput Vis, 1994, 13: 229–251
13 Paragios N, Deriche R. Geodesic active regions and level set methods for supervised texture segmentation. Int J Comput Vis, 2002, 46: 223–247
14 Shen C, Yu H, Liu X, et al. Medical image segmentation based on level set with new local fitting energy. In: Proceedings of IEEE Conf on Medical Image Analysis and Clinical Applications. Los Alamitos: IEEE Computer Society Press, 2010. 34–37
15 Chiu Y J, Pham V T, Tran T T, et al. Evaluation of active contour on medical inhomogeneous image segmentation. In: Proceedings of IEEE Conf on Computer Science and Information Technology. Los Alamitos: IEEE Computer Society Press, 2010. 311–314
16 Zhang K, Song H, Zhang L. Active contours driven by local image fitting energy. Pattern Recognit, 2010, 43: 1199–1206
17 Mao H, Liu H, Shi P. Neighbor-constrained active contours without edges. In: Proceedings of IEEE Conference on Computer Vision and Pattern Recognition Workshops. Los Alamitos: IEEE Computer Society Press, 2008. 1–7
18 Chen Y, Zhang J, Macione J. An improved level set method for brain MR images segmentation and bias correction. Comput Med Imaging Graph, 2009, 33: 510–519
19 Zhai Y, Wu B, Zhang D, et al. A new variational model for segmenting objects of interest from color images. Math Probl Eng, 2010, 2010: 1–16
20 Boykov Y Y, Jolly M P. Interactive graph cuts for optimal boundary & region segmentation of objects in n-d images. In: Proceedings of IEEE Int Conf on Computer Vision. Los Alamitos: IEEE Computer Society Press, 2001. 105–112
21 Grady L. Random walks for image segmentation. IEEE Trans Pattern Anal Mach Intell, 2006, 28: 1768–1783
22 Xiang S, Nie F, Zhang C, et al. Interactive natural image segmentation via spline regression. IEEE Trans Image Process, 2009, 18: 1623–1632
23 Xiang S, Nie F, Zhang C. Semi-supervised classification via local spline regression. IEEE Trans Pattern Anal Mach Intell, 2010, 32: 2039–2053
24 Mao H, Liu H, Shi P. A convex neighbor-constrained active contour model for image segmentation. In: Proceedings of Int Conf on Image Processing. Los Alamitos: IEEE Computer Society Press, 2010. 793–796
25 Nikolova M, Esedoglu S, Chan T F. Algorithms for finding global minimizers of image segmentation and de-noising models. SIAM J Appl Math, 2006, 66: 1632–1648